PERGAMON

International Journal of Heat and Mass Transfer 43 (2000) 281–296

International Journal of HEAT and MASS TRANSFER

www.elsevier.com/locate/ijhmt

Pressure and power generation during explosive vaporization on a thin-film microheater

Z. Zhao, S. Glod, D. Poulikakos*

Institute of Energy Technology, Laboratory of Thermodynamics in Emerging Technologies, Swiss Federal Institute of Technology, ETH Center, Zurich 8092, Switzerland

Received 19 August 1998; received in revised form 9 March 1999

Abstract

When a liquid is superheated above its boiling point to temperatures near or at the homogeneous nucleation limit, the energy released could create a so-called explosive vaporization, if a significant fraction of this energy is manifested in the form of vapor expansion. In this study, a thin-film microheater (100 μm × 110 μm) was placed on the underside of a water layer. The surface temperature of the heater was rapidly (6 μs) raised electrically, well above the boiling point of water. As a result, rapid vaporization took place. Due to its rapid growth, the vapor volume performs mechanical work on its surrounding and emits acoustic pressure waves. By measuring the acoustic emission from an expanding volume, the dynamic growth of the vapor microlayer is reconstructed where a linear expansion velocity up to 17 m/s was reached. Using the Rayleigh–Plesset equation, an absolute pressure inside the vapor volume of 7 bar was calculated from the data of the acoustic pressure measurement. The amount of extractable mechanical energy produced from the explosive expansion of a vapor microlayer on a thin-film microheater surface, its rate of production, and the energy conversion efficiency was also quantified in this work.

1. Introduction

A *vapor explosion* is a physical event in which the volume of vapor phase expands at a maximum rate in a volatile liquid. Rapid introduction of energy into the volatile liquid is necessary to initiate and sustain the vapor volume growth at the high rate; in doing so, the liquid vaporizes at high pressures and expands, performing work on its surroundings. In contrast to large scale vapor explosions of the kind that can be encountered in nuclear powerplant accidents [1], the microscopic explosive vaporization considered herein is generated by rapid heating of a liquid with microheaters, is controllable electronically and can be used as a highly localized energy source in a host of emerging technologies involving thermal micromechanical systems. A case in point is the commercial success of thermal ink-jet (TIJ) printers. The key to the thermal ink-jet technology is the action of exploding micro bubbles, which propel tiny ink droplets through the openings of an ink cartridge.

Despite current commercial success of the TIJ technology, our knowledge of the *explosive vaporization process* at the microscopic level on a heated surface is limited. The energy released when a liquid nucleates at high intensity could create a so-called *vapor explosion* if a significant fraction of the heating energy appears

* Corresponding author. Fax: +41-1-6327858.
E-mail address: poulikakos@ltnt.iet.mart.ethz.ch (D. Poulikakos)

0017-9310/00/$ - see front matter
PII: S0017-9310(99)00129-5

Nomenclature

A	interface surface area
c	speed of sound in the liquid
E_a	acoustic energy
h_{lv}	heat of vaporization
k	thermal conductivity
M	molecular weight
p_g	initial bubble pressure
p_l	transient pressure wave in the liquid
p_o	ambient liquid pressure
p_s	bubble pressure at large time
p_v	vapor pressure within the bubble
Q	thermal energy
q''_{Heater}	heat flux from microheater
q''_{max}	theoretical upper limit of heat flux
R	bubble radius
R_e	electric resistance of thin-film microheater
t	time
T^*	liquid superheat limit
t_c	delay time between start of heating pulse and first pressure peak
T_l	liquid temperature
t_p	duration of voltage pulse
T_s	liquid saturation temperature
T_v	vapor temperature
V	volume
V_e	electric pulse voltage
V_o	initial volume of vapor layer
W	mechanical work
x	distance from heater to sensor

Greek symbols

α	thermal diffusivity
η	efficiency
η_a	acoustic conversion efficiency
μ_l	liquid viscosity
ρ_l	liquid density
ρ_v	vapor density
σ	liquid surface tension
τ	dummy integration variable
Ω	number of pre-existing nuclei per unit area

in form of rapid vapor expansion. Microscopic vapor explosions have been generated by heating liquids rapidly with microheaters [2–5] and high energy laser beams [6–9].

The kinetic energy from rapidly expanding microbubbles can, in principle, be utilized to drive micromechanical systems. Successful extraction of the work from the high-pressure pulses generated by the microscopic vapor explosions could revolutionize the design and application of thermal micromachines in situations where significant levels of force are required.

Previous investigations of vapor bubble generation and growth on thin-film micro heaters are largely focused on the incipience conditions of the microscopic boiling explosion [10–12] and the liquid motion induced by the rapid oscillation of growth and collapse of vapor micro layers [11,13]. In an effort to develop bubble-jet printers, a series of studies were carried out by Asai et al. and Asai [5,10,13–15]. They concluded that the bubble generation mechanism in the bubble jet recording process is due to the spontaneous nucleation of ink vapor followed by instantaneous film boiling and eventual cavitation bubble collapse, which is realized by short heating pulses with an extremely high heating rate of approximately 3×10^8 K/s^{-1} [5]. A theoretical treatment was proposed and later refined by Asai [13–15] to predict the bubble behavior after the occurrence of homogeneous nucleation. In Asai's model, the bubble pressure, p_v, was represented by an impulsive function:

$$p_v = (p_g - p_s)\exp[-(t/t_0)^{1/2}] + p_s \quad (1)$$

where p_g is the initial bubble pressure, p_s the bubble pressure at large time, t the time after the onset of homogeneous nucleation, and t_0 is a time constant. The initial bubble pressure, p_g, and the time constant, t_0, have to be chosen for different ink compositions and heater geometry so that the calculated drop velocity agrees with the experiments.

Existing numerical simulations of the *bubble growth and collapse* cycle and bubble oscillation-induced liquid flow begin with the formation of a vapor sheet over the surface of thin-film microheaters [10,11,13,16,17]. The expansion of the vapor film sets the liquid in motion. During the expansion, the pressure within the vapor film was assumed to follow either the ideal gas law [10,11,16] or an impulsive function such as Eq. (1) [16,17]. Because of the lack of experimental data on pressure transients within an exploding microbubble, the value of the initial pressure is usually ascribed to be the saturated vapor pressure at the temperature of boiling incipience. It was speculated that the spontaneous nucleation temperature of microheaters in thermal ink jet printers is in the range from 270 to 300°C [10,12,13]. The corresponding saturated vapor pressure varies from 55 to 86 bar. This large variation

in ascribed bubble initial pressure can substantially alter the predicted bubble dynamics during the growth and collapse cycles, raising doubts about the simulated behavior for both bubble and liquid. Furthermore, no experimental confirmation of either Asai's model, Eq. (1), or the ideal gas model for the pressure variation of an exploding microbubble has yet been attempted.

The fluid dynamics and thermodynamics of microscopic vapor explosion are indeed complicated during both the initiation, propagation and collapse stages. Inconsistent findings and conclusions have been reported in the literature for the mechanism of initiation of microscopic vapor explosion [5,11,16,18–20]. Inconsistency exists among experimental measurements of the maximum fluid temperatures reached before explosive vaporization on microheaters. Existing theories and models do not predict the development of the thermodynamic parameters, such as temperature and pressure, during microscopic vapor explosion. A generally accepted theory has yet to be devised to predict the mechanisms that govern micro-scale vapor explosion. Neither the total energy nor the theoretical limits of the amount of useful work generated by the microscopic vapor explosions are sufficiently explored. The present work attempts to provide quantitative measurements of the pressure transients generated from an exploding microbubble and to quantify the amount of mechanical work released (transferred) into the surrounding liquid from this phenomenon.

2. Experiment

2.1. Thin-film microheater

According to Skripov [21], the liquid heating rate has to be high enough for explosive boiling to occur on a heat-releasing surface. To obtain a high heating rate, the thermal mass of a heater should be as small as possible. This can be conveniently achieved with microscopic thin-film heaters of sub-micron thickness deposited on a substrate with low thermal conductivity. For the present study, thin-film microheaters from a commercial thermal ink jet printhead (HP 51604A Ink Cartridge, Hewlett-Packard) were used to perform the experiments.

The resistor chip in a new thermal ink jet printhead is removed to expose the thin-film microheaters (Fig 1(a)). The microheater (resistor) structure is fabricated on a glass substrate (fused silica) using standard IC processing techniques [22]. To prevent diffusion of impurities from the glass into the resistor and conductor films, a dielectric material such as sputtered silicon dioxide is deposited first on the glass substrate. The material of the resistor film is tantalum–aluminum. It is covered with corrosion-resistant passivation and protective layers. The conductor film is deposited by magnetron sputtering of aluminum doped with copper. To improve the electrical contact reliability and the electrical conductance, the conductor path is further coated with nickel and gold layers. The dimension of the resistor films were measured with an optical microscope (Olympus BX60). The microheater length along the electrical conduction path is 110 μm and the width is 100 μm, (Fig. 1(b)). The electric resistance of the conductors leading to the array of microheaters on the TIJ chip is $5.6 \pm 0.1\ \Omega$. The variation is principally due to the difference in the length of conductive path. The electrical resistance over a resistor circuit measured between the connection pads of the conductors on the TIJ chip is $66.2 \pm 3.9\ \Omega$. The difference between the above two measurements yields $60.6 \pm 4.0\ \Omega$ for the value of the microheater electric resistance, R_e.

The thermal energy, Q, produced in a thin-film microheater during the application of a square electrical voltage pulse, V_e, on the heater can be calculated

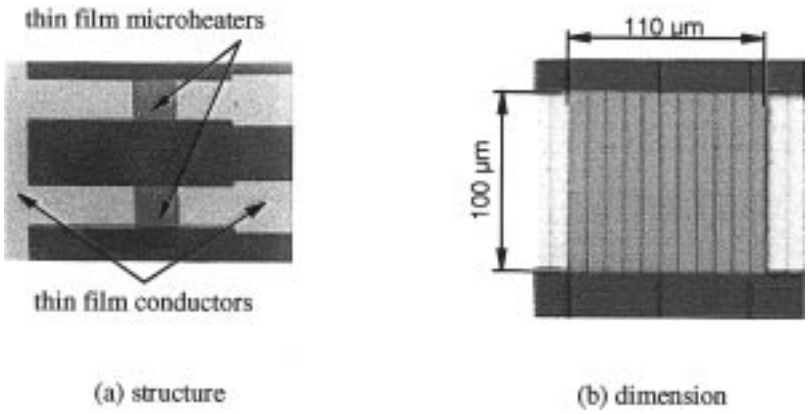

Fig. 1. Thin-film microheater from a TIJ chip.

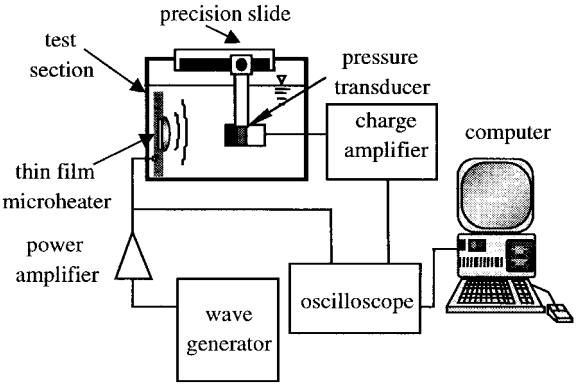

Fig. 2. Schematic of pressure transient measurement.

by

$$Q = \frac{V_e^2}{R_e} t_p \tag{2}$$

where t_p is the duration of the voltage pulse. For a typical pulse of 25 V and 6 μs in the experiment, the total heat generation on the microheater is about 62 μJ and the power flux is of the order of 1 GW/m^2 on the microheater surface.

2.2. Experimental setup

The apparatus for the measurement of the acoustic pressure wave generated from a thin-film microheater is shown schematically in Fig. 2. A square voltage pulse with a preset duration is generated by a wave generator (LW420 Arbitrary Waveform Generator, LeCroy SA, Geneva, Switzerland). The voltage of the square pulse is amplified through the power amplifier into a dc voltage pulse with preset pulse amplitude. The dc voltage pulse is then applied to the thin-film microheater and recorded by the storage oscilloscope (LC334A, 500 MHz Digital Storage Oscilloscope, LeCroy SA, Geneva, Switzerland). The acoustic pressure wave emitted from the microheater surface is measured by a pressure transducer (Kistler quartz pressure sensor for high frequency 603B, Kistler Instrumente AG, Winterthur, Switzerland) mounted on a precision slide and facing the surface of the thin-film microheater. The pressure transducer generates an electrostatic charge signal corresponding to the received pressure signal. This signal is transformed into a voltage signal, amplified by the charge amplifier (Type 5007 Charge Amplifier, Kistler Instrumente AG, Winterthur, Switzerland) and recorded by the oscilloscope. The recorded data is transferred from the oscilloscope to a personal computer for analysis. In an experiment, both the microheater and the pressure transducer are immersed in water that is open to the atmospheric pressure. The dimensions of the container are 130 × 70 × 30 mm and the water is filled in to a height of 25 mm.

The choice of the pressure sensor is based on its ability to resolve the details of the acoustic pressure wave and to record the peak pressure values. Pressure sensors with response frequency from 2 MHz [23] to 10 MHz [24] were used in two previous investigations to study the explosive boiling on microheaters. Based on the time scale of the two characteristic pressure peaks reported in these two studies, the fundamental frequency of the acoustic pressure waves emitted from the explosive boiling on a microheater is estimated to be in the range from 100 to 200 kHz. The pressure transducer used in the present study has a natural frequency of 400 kHz and was calibrated for pressure range up to 200 bar by the manufacturer. The transducer diaphragm has a diameter of 5.55 mm. This model of pressure transducer was reported to be able to record the acoustic pressure waves produced from the explosive boiling of a butane droplet at its superheat limit temperature by different groups [25,26].

A similar setup is used to visualize the explosive vaporization. The heater pad is put under a microscope (Olympus BX60) with 50 times magnification and is covered with a water film of approximately 400 μm. A CCD camera (Pulnix TM795) mounted on the microscope records the boiling process. A Xenon flash lamp (Hamamatsu L4634), synchronized with the heating pulse signal, is controlled by a delay unit that allows the CCD camera to capture individual bubble images at various stages of the boiling process. The images are discussed in the following section and mapped to the corresponding point on the pressure trace of acoustic measurement.

3. Results

3.1. Acoustic pressure waves produced by the microscopic explosive boiling

Bubbles are a source of acoustic emission. When a bubble entrained in a liquid undergoes expansion or contraction, acoustic pressure waves are radiated from the bubble surface [27]. This pressure is called acoustic pressure. The pressure produced within the vapor micro layer during microscopic vapor explosion provides the 'driving force' for the motion of the bulk liquid. The pressure transient propagates from the vapor region into the surrounding liquid through the interface between vapor and liquid. The intensity of the acoustic pressure waves represents the intensity of the microscopic vapor explosion on the microheater surface. Therefore, the dynamic interaction between the exploding vapor micro layer and the surrounding

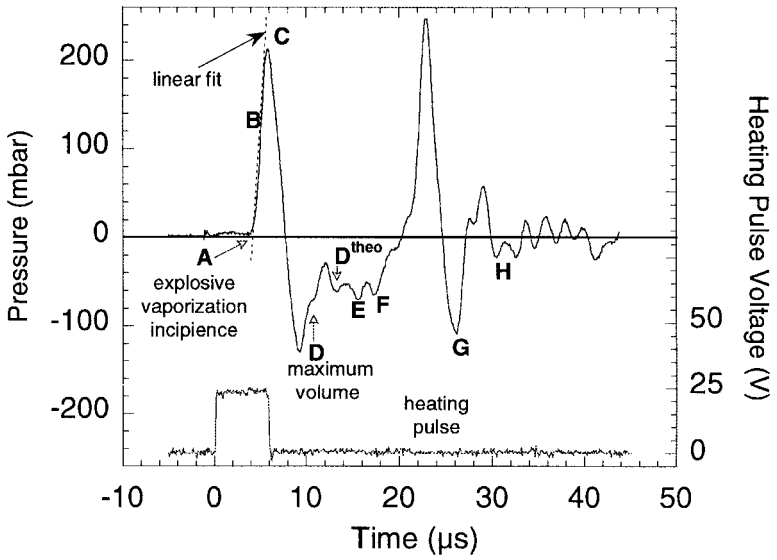

Fig. 3. Acoustic pressure wave produced by a square voltage heating pulse. Heating pulse. Voltage = 25 V, duration = 6 μs, transducer to microheater distance $x = 1$ mm.

liquid can be characterized by measuring the acoustic pressure wave in the liquid during the process of sequential growth and collapse of the vapor region.

Fig. 3 shows a typical acoustic pressure graph produced by the explosive boiling of water on a thin-film microheater measured at transducer to microheater distance $x = 1$ mm. The heating is provided by a 25 V and 6 μs square voltage pulse, which is also shown in Fig. 3. Because of the short heating pulse duration, the acoustic pressure wave produced from one heating pulse is not affected by a previous pulse for heating pulse frequency up to 80 Hz [28] at $x = 1$ mm. At heater to sensor distance $x = 10$ mm, the acoustic signal is not affected for heating pulse frequencies up to 500 Hz. The frequency of the heating pulses to the microheater is 5 Hz in the present experiment. The recorded oscillogram covers the first 50 μs after the arrival of a heating pulse in the measurements.

As shown in Fig. 3, the acoustic pressure waveform from the explosive vaporization on the microheater is characterized by two positive pressure pulses with each of them immediately followed by a negative pressure pulse. The first positive pressure pulse corresponds to the generation and expansion of a vapor microlayer on the microheater, which launches a compression wave into the surrounding liquid. The second positive pressure pulse is generated after the implosion of the contracting vapor layer and is the result of regrowth (rebounding) of the vapor bubble. The symbol 'A' indicates the location on the acoustic waveform where the explosive vaporization begins, the symbol 'C' represents the location of the first pressure peak. The letters A–H on the acoustic trace correspond to the stages when the images of (A)–(H) in Fig. 4 were taken. As shown in Fig. 4(C) the bubble is still growing at this moment. The symbol 'D' in Fig. 3 corresponds to the point where the vapor microlayer reaches a maximum volume as a result of the explosive vaporization. The theoretical method to locate the initiation point 'A' and the point when the maximum vapor volume is reached will be discussed in the next section.

The waveform of the acoustic pressure in Fig. 3 is consistent with the acoustic pressure trace reported by Meyer [24] for the explosive boiling of water on a microheater. The positive and negative values of the acoustic pressure wave correspond to the acceleration ($d^2V/dt^2 > 0$) and deceleration ($d^2V/dt^2 < 0$), respectively, of the vapor volume growth (Fig. 3). After the initiation of the explosive vaporization at 'A', the acoustic pressure increases sharply (region 'B') until the peak of the first positive pressure pulse, 'C', where the acceleration rate of the vapor volume growth reaches a maximum. These are the initial stages of vapor microbubble rapid generation and growth. Detailed pictures of the bubbles during these states are shown in Fig. 4(A)–(C).

Fig. 4(A) shows that vapor pockets are formed at 'preferential' sites on the microheater surface. In addition, the gray scale (brightness) on the heater surface is no longer as uniform as the gray scale before the application of the heating pulse. Due to the optical limitation of the microscope, we are not able to determine from the visualization images whether a very thin layer

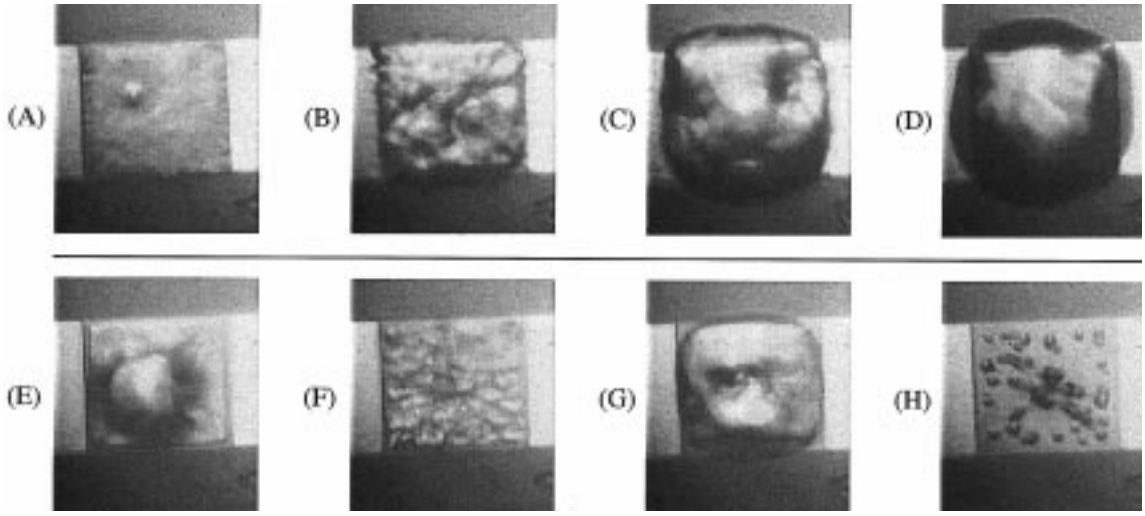

Fig. 4. Progressive stages of explosive vaporization on a thin-film microheater. (A) Incipience. (B) Formation of single bubble. (C) Bubble still growing, starts decelerating. (D) Maximum bubble volume. (E) Bubble shrinks and breaks up. (F) Beginning of bubble regrowth. (G) Maximum bubble volume for regrowth. (H) Bubble dissipates into small bubbles.

(on the order of sub micrometer) of vapor was formed on the heater surface. The vapor pocket sites increase rapidly and connect with each other into a thin layer of vapor blanket over the microheater surface, Fig. 4(B). An explosive expansion of the vapor layer immediately follows and accelerates with a roughening bubble interface, Fig. 4(C).

It should be noted here that due to the resolution limit of the optical imaging system, surface objects smaller than 2 μm on the thin-film microheater cannot be clearly identified. Nevertheless, the obtained microscopy images captured the features of the explosive vaporization process on microheater surface that are very different from the traditional pool boiling process during the early stages of the vapor generation and growth. With the continuing expansion of the vapor volume after the end of the heating pulse, the acoustic pressure rapidly decreases to values below ambient pressure and reaches the peak of the first negative pulse (Fig. 3) where the deceleration rate of vapor expansion is at its maximum. The expansion of the bubble slows down and eventually reaches a maximum volume, as indicated by 'D' in Fig. 3, before it starts to shrink and collapse on the microheater surface at 'E'. The corresponding images of the bubble are visualized in Fig. 4(D) and (E). The collapsing bubble breaks up into smaller bubbles on the heater surface as the surrounding liquid accelerates towards the vapor layer ($d^2V/dt^2 < 0$) and crushes the bubble. The smaller bubbles regrow immediately after the break up, Fig. 4(F), and coalesced into a single bubble of comparable size as the initial bubble before break up, Fig. 4(G). The 'rebound' bubble breaks up again on the microheater surface, Fig. 4(H). The rebound of the smaller bubbles after 'F' causes rapid vapor expansion in the region, which emits a second compression wave that has a slightly higher peak value than the first positive peak at 'C' (Fig. 3). Based on the assumption of inviscid and incompressible fluid, Rayleigh considered the collapse of a spherical bubble in an infinite fluid and developed the now well-known implosion mechanism of cavitation whereby extremely high pressures are generated during the last moment of bubble collapse [29].

It has been shown since the experiments by Pavlov et al. [30,31] and Skripov et al. [2,32] that microscopic vapor explosion can be initiated and contained locally on a microheater by pulsatory heating at very high rate. The measured boiling incipience temperature is usually at or close to the kinetic limit of homogeneous nucleation [2,30–34]. According to Skripov [21], for transient processes with a fast input of heat into the system or upon an abrupt drop in the external pressure, superheating of the liquid continues in spite of the action of heterogeneous vaporization sites. Under these conditions the purity of the system does not play the governing role. When there is a shortage of preexisting nuclei the explosive nucleation mechanism within the microheater thermal influence zone can operate as the heat-runoff regulator that prevents further temperature increase. Therefore a threshold value of heating rate should exist for a given liquid and heating surface above which microscopic vapor explosion can be realized. The criterion given by Skripov for the spontaneous nucleation to dominate is

$$\frac{dT}{dt} > \pi\Omega\alpha(T^* - T_s) \quad (3)$$

where dT/dt is the rate of temperature rise, Ω the number of pre-existing nuclei per unit area on the heating surface, α the liquid thermal diffusivity, T^* the superheat limit of the liquid, and T_S the saturation liquid temperature. The condition to realize the spontaneous nucleation on the heating surface was reported to be $dT/dt > 6 \times 10^6$ K/s^{-1} for water heated by a platinum wire under the atmospheric pressure and at a Ω value of 10^6 cm^{-2} [21]. Direct measurement of the liquid temperature rise rate is difficult [35], which makes the application of the criterion of Eq. (3) in experiments intractable. Since the liquid heating rate is primarily determined by the applied heating voltage in the present experiment, the effect of heating rate on the explosive boiling process can be probed by comparing the acoustic pressure emissions from the exploding microscale vapor layers for different amplitude of heating pulses with fixed duration.

Fig. 5 shows the acoustic waves generated from heating pulses at three different voltages. The heating pulse duration was 6 μs as indicated by the shaded area in Fig. 5. It is immediately clear that with the reduction of the heating pulse voltage from 37 V in Fig. 5(a) to 25 V in (b) and 19 V in (c) the amplitude of the acoustic pressure is reduced for both the first and the second positive acoustic pulses. The amplitude of the higher frequency oscillations following these two pulses is also reduced with the decrease of the heating pulse voltage. Other than the reduction of oscillation amplitudes and a slight decrease in the time delay between the peak of the two positive pulses, the shapes of the acoustic traces are quite similar in Fig. 5(a) and (b). In Fig. 5(c), the amplitude of acoustic oscillation at higher frequencies is very small between the peaks of the two positive pulses such that the pressure trace appears 'smooth' in this section of the curve. The lack of higher frequency oscillations between the two positive pulses of the acoustic pressure trace in Fig. 5(c) suggests that the vapor layer dynamics on the microheater at the 19 V heating pulse is different than that under the higher heating rates in Figs. 5(a) and (b), in the range where the explosive growth approaches the maximum volume and the entire phase of subsequent volume collapse.

A liquid has to be superheated in order to boil explosively. The ability to superheat a liquid far beyond its thermodynamic equilibrium temperature of vaporization is dependant upon the liquid heating rate on a heat-releasing surface. According to Skripov's criterion, Eq. (3), a threshold heating rate value should exist for a given liquid and heating surface above which explosive boiling can be realized. For water and the thin-film microheater heated by a 6 μs square

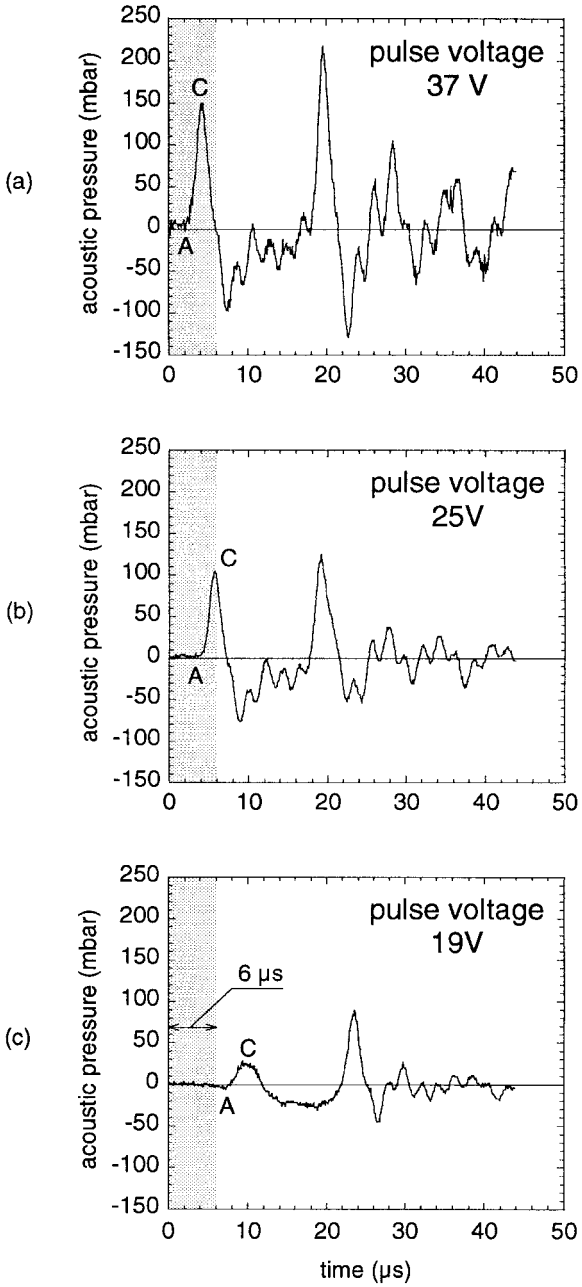

Fig. 5. Acoustic waveform generated at different voltages of heating pulse. Heating pulse duration = 6 μs, transducer to microheater distance x = 2 mm.

shape voltage pulse in the present experiment, the minimum heating pulse voltage is 18.6 V below which no acoustic emission was detected [36]. The heating rate effect on the amplitude of acoustic emission is plotted in Fig. 6(a). The heating rate effect on the delay time, t_c, between the start of the heating pulse and the peak of the first positive acoustic pulse, 'C', is

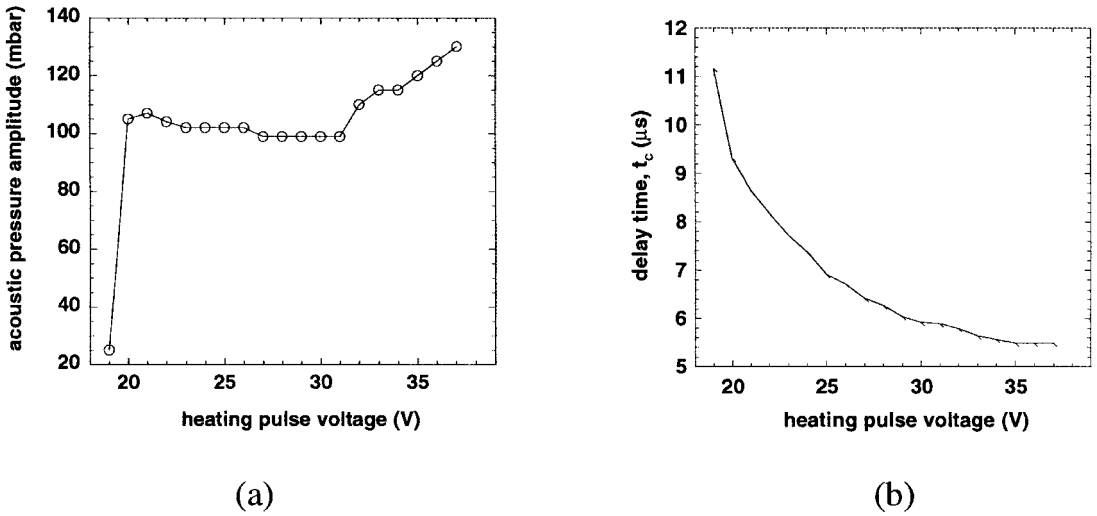

Fig. 6. (a) The amplitude and (b) the delay time at the peak, 'C', of the first positive acoustic pressure pulse under various heating pulse voltages. Heating pulse duration = 6 μs, transducer to microheater distance x = 2 mm.

plotted in Fig. 6(b). It is very interesting to note that the amplitude of the first positive pulse, 'C', remains nearly constant over a large range of applied voltage from 20 V to 31 V (Fig. 6(a)), while the delay time between the start of voltage application and the arrival of the first positive peak of the acoustic pressure decreases monotonically with the increase of heating pulse voltage (Fig. 6(b)). The amplitude of the first positive pulse, 'C', increases again with the increase of heating pulse voltage above 31 V (Fig. 6(a)).

The initially insensitive response of acoustic emission from the vapor volume explosive growth with the increase of energy input (Fig. 6(a)) can be advantageous in stabilizing the operation conditions for micro electromechanical systems, such as the thermal ink jet printer that draws the driving force from the exploding vapor microlayer.

In the present paper, we focus on the pressure inside the bubble and the available mechanical work generated from the explosive vaporization process. It is necessary to quantify these parameters in order to realize the engineering of mechanical microdevices. A detailed study on the initiation processes of the microscopic vapor explosion will be the subject of a subsequent investigation.

3.2. The Schrage heat flux condition for vapor explosion

The theoretical upper limit of heat flux, $q''_{\max}$, that can conceivably be achieved in a vaporization or condensation process was given by Schrage [37,38]

$$q''_{\max} = \rho_v h_{lv} \left(\frac{RT_v}{2\pi M} \right)^{1/2}, \tag{4}$$

where ρ_v is the vapor density, T_v the temperature of vapor, h_{lv} the heat of vaporization or condensation, M the molecular weight, and R = 8.314 J/(mole K) is the universal gas constant. The above equation is derived for a planar interface between vapor and liquid, from the kinetic theory of gases assuming that all the molecules pass through the interface in one direction and no molecules return to the interface. For water at atmospheric pressure, a value of $q''_{\max} = 223$ MW/m^2 is predicted from the above equation for the maximum heat flux through a vapor/liquid interface.

Under constant heat flux condition, the transient temperature distribution on the surface of a semi-infinite wall is [39]

$$T_w = \frac{2q''_{\text{Heater}}(\alpha t/\pi)^{1/2}}{k}. \tag{5}$$

Since the microheater thickness is on the order of 1 μm, the temperature variation across the thickness of the thin-film is very small. If we assume that the temperature of the glass substrate in contact with the thin-film microheater is the same as the water temperature in contact with the microheater, it is estimated from the above equation that approximately 45% of the total heat flux generated from thin-film microheater will go into water. At a heating pulse voltage of 37 V, the heat flux into the water layer is about $q''_{\text{Heater}} = 945$ MW/m^2 which is more than four times higher than the theoretical upper limit of interface heat flux. As demonstrated in Fig. 7, which illustrates a small portion of the near heater region at the beginning of the nucleation process, if the applied heat flux, q''_{Heater}, is equal or greater than the theoretical upper limit of interface heat flux,

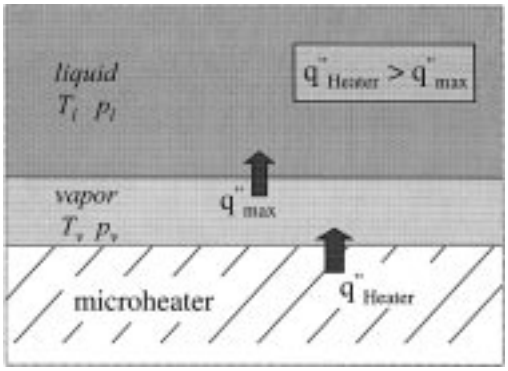

Fig. 7. Vapor explosion condition.

$$q''_{\text{Heater}} \geq \rho_v h_{lv} \left(\frac{RT_v}{2\pi M} \right)^{1/2}, \tag{6}$$

the liquid temperature in contact with the heat-releasing surface will continue to rise until the explosive vaporization occurs. This is because the heat transfer rate through vaporization at pre-existing nucleation sites will not be high enough to remove the heat flux imposed by the microheater. According to Eq. (6), the minimum voltage applied to the thin-film microheater that can generate explosive vaporization is approximately 18 V. It should be noted that Eq. (6) represents a sufficient condition to generate an explosive vaporization if the heating duration is long enough for vapor explosion to develop. The heat flux to generate explosive vaporization could be lower. However, if the development time is sufficiently shorter than required for the explosive growth of vapor phase (i.e. very short heating pulse), explosive vaporization may not develop even when Eq. (6) is satisfied.

3.3. Bubble dynamics and conversion of extractable mechanical energy

Due to the complexity in the interactions between vapor phase and its surrounding liquid, a universal relation describing the vapor phase growth in a liquid and the dynamic response of the surrounding liquid has yet to be established. This dynamic interaction is further complicated when it occurs near or on a solid wall. Our current understanding has been based on highly idealized conditions such as for a single oscillating gas volume with perfectly smooth surface undergoing expansion or contraction in an unbounded liquid [21,40,41]. Under these idealized conditions, the acoustic pressure wave in the liquid, p_l, emitted by the growing vapor volume, V, at a distance of r from the source in the liquid is given by [42]

$$p_l(r, t) - p_o = \frac{\rho_l}{4\pi r} \frac{d^2 V(t - r/c)}{dt^2}, \tag{7}$$

where p_0 is the ambient liquid pressure surrounding the source, t the time, ρ_l the liquid density, and c the speed of sound in the liquid. In addition to the above-mentioned assumptions, application of Eq. (7) requires that the wavelength, λ, of the acoustic pressure wave and the distance r must be large compared to the characteristic length, R, of the vapor volume (λ and $r \gg R$) such that the bubble behaves as a compact sound source. For a given distance in a liquid, the pressure is therefore proportional to the acceleration with which the vapor phase grows. The vapor volume growth velocity as well as the volume itself can be obtained by integrating Eq. (7),

$$\frac{dV(t - r/c)}{dt} = \frac{4\pi r}{\rho_l} \int_0^t p_a(r, \tau)\, d\tau, \tag{8}$$

and

$$V(t - r/c) = \int_0^t \frac{dV(\tau - r/c)}{d\tau}\, d\tau, \tag{9}$$

where $p_a(r,t) = p_l(r,t) - p_0$ is the measured acoustic pressure. If a further assumption of a perfectly spherical bubble is made for the shape of the vapor layer generated on a thin-film microheater surface, the bubble radius, R, can be calculated from

$$R(t) = \left(\frac{3V(t)}{4\pi} \right)^{1/3}. \tag{10}$$

It is unlikely that the vapor layer on the microheater surface will be in spherical shape with a perfectly smooth bubble wall. Nevertheless, the bubble radius as defined by Eq. (8) represents the length scale of the vapor volume during the explosive vapor growth. Under the above assumptions, the movement of the idealized bubble wall is related to the vapor pressure within the bubble, p_v, by the classical Rayleigh–Plesset equation [43],

$$p_v(t) - p_0 = \rho_l R \frac{d^2 R}{dt^2} + \frac{3}{2} \rho_l \left(\frac{dR}{dt} \right)^2 + \frac{4\mu_l}{R} \frac{dR}{dt} + \frac{2\sigma}{R}, \tag{11}$$

where μ_l is the liquid viscosity and σ the liquid surface tension.

The incipience point, 'A', of explosive vaporization on the measured acoustic waveform of pressure in Fig. 3 can be located from the theory of inertially controlled bubble growth. After the nucleation of vapor bubbles on a heat-releasing surface, the initial stage of vapor volume growth is limited by the surface tension force. With the growth and, most likely, coalescence of vapor bubbles, the pressure threshold needed to over-

come the surface tension will be reduced rapidly and explosive vaporization will occur on the surface. It is assumed that the explosive vapor volume growth is limited only by the surrounding liquid inertia, in which the vapor volume increases at a maximum rate with time

$$V(t) = V_0 t^3 \tag{12}$$

where V_0 is the initial volume of vapor layer at the beginning of the inertially controlled vapor growth. This relation defines the process of explosive vaporization. Substituting the above equation into the equation for acoustic pressure, Eq. (7), yields

$$p_a(r, t) = \frac{3V_0\rho_l}{2\pi r} t. \tag{13}$$

The acoustic pressure emitted from microscopic vapor explosion is a linear function of time immediately after the incipience of vapor explosion. Eq. (13) is used in Fig. 3 to locate the incipience of explosive vaporization by curve fitting the growth part of the first positive acoustic pulse. The linear fit is chosen for the curve section between 5 and 95% of the pressure at the peak 'C'. The intersection point, 'A', between the line fit and the zero acoustic pressure $p_a(t) = 0$ is defined as the incipience point of explosive vaporization in this paper. The maximum variation of the incipient time of explosive vaporization, t_A, is 0.1 μs between curve fitting in the full range of pressure rise to 'C' and in the range of 10–90% of the pressure at 'C' for all the experiment runs.

As a bubble expands or contracts in a liquid, mechanical work is transferred between the bubble and the surrounding liquid. The kinetic energy transferred from the expanding vapor microlayer on a thin-film heater surface can be used, in principle, to drive electromechanical microdevices such as micro actuators and pumps. Information about the useful work converted from the thermal energy on the surface of a microheater is critical for these applications. The mechanical work, $E_m(t)$, done by a vapor volume on the surrounding liquid is

$$E_m(t) = \int p_v \, dV = \int_0^t p_v \frac{dV(t)}{dt} \, dt, \tag{14}$$

where the pressure within a bubble is calculated from Eq. (11) and the volume velocity dV/dt from Eq. (8). Part of the mechanical work is used to overcome the ambient pressure and to increase the vapor/liquid interface surface area. Hence, it is not available as useful energy. The useful mechanical work, $W(t)$ that can be extracted from the explosive vapor expansion is given by

$$W(t) = \int_0^t p_v \frac{dV(t)}{dt} \, dt - \int_0^t p_0 \frac{dV(t)}{dt} \, dt - \int_0^t \sigma \frac{dA(t)}{dt} \, dt \tag{15}$$

where $A(t)$ is the interface surface area. If the vapor layer surface area can be approximated by the surface area of a spherical bubble with the same volume, the extractable mechanical work can be calculated from

$$W(t) = \int_0^t \left[p_v - p_0 - \sigma \left(\frac{32\pi}{3V(t)} \right)^{1/3} \right] \frac{dV(t)}{dt} \, dt \quad \text{(J)}. \tag{16}$$

The corresponding power is the integrand in the above integration,

$$\frac{dW(t)}{dt} = \left[p_v - p_0 - \sigma \left(\frac{32\pi}{3V(t)} \right)^{1/3} \right] \frac{dV(t)}{dt} \quad \text{(W)}. \tag{17}$$

The total acoustic energy radiated by an omnidirectional acoustic source on a surface, E_a, can be obtained by integrating the acoustic power over the time [44]

$$E_a = \frac{2\pi r^2}{\rho_l c} \int p^2 \, dt, \tag{18}$$

The sound speed, c, of 1481 m/s in water at 20°C is used in the above calculations.

Fig. 8 shows the vapor microlayer dynamics reconstructed from the measured acoustic pressure waves in Fig. 5 based on the above theory. The vapor incipience points defined in the previous section and the vapor volume maximums reached are denoted with arrows in Fig. 8 for each of the three different tests. At a given duration of voltage heating pulse (6 μs), the maximum volume of the vapor microlayer increases with the increase of the heating pulse voltage up to 3.15×10^{-12} m^3 for the 37 V heating pulse (Fig. 8(a)). The maximum volume expansion velocity increases with the increase of applied heating pulse voltage (Fig. 8(b)). The incipience time of the explosive vaporization decreases with the increase of the heating pulse voltage. After expanding to the maximum volume, the vapor microlayer shrinks and will eventually contract to a minimum volume just before bubble rebound or break-up. It is well known that a collapsing vapor bubble may disintegrate into clouds of smaller bubbles near the end of bubble collapse due to the development of Rayleigh–Taylor instability [43,45,46]. Bubble disintegration at the end of the bubble collapse was observed in our visualization study, Fig. 4(E) and (F). As a result, the compact sound source assumption made in Eq. (7) is not satisfied during the later stages of vapor volume contraction prior to the bubble regrowth. The results presented in Figs. 8–11 cover the time period from the beginning of joule heating at

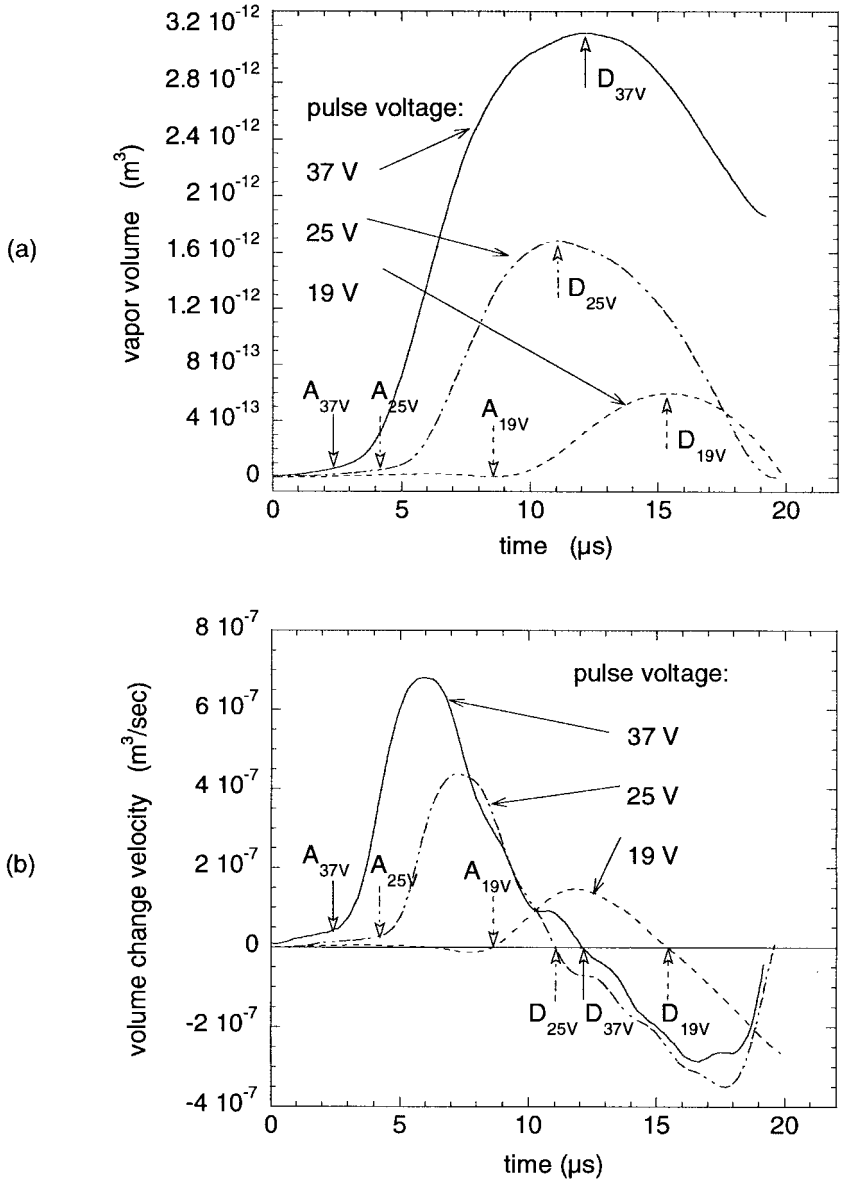

Fig. 8. Vapor microlayer growth dynamics. (a) vapor volume and (b) volume velocity. Symbols 'A's' and 'D's' refer to the points of explosive vaporization incipience and vapor volume at maximum, respectively. The subscripts represent the corresponding heating pulse voltage. Heating pulse duration = 6 μs.

least up to the maximum vapor volume (symbol 'D' in Fig. 8). The present experiment is primarily concerned with the explosive growing phase of the vapor microlayer and the associated energy transfer process. It will be of interest to measure the minimum size of vapor volume before bubble disintegration occurs. However, the current acoustic measurement cannot resolve the onset of bubble disintegration. Therefore, the minimum vapor volume just before bubble disintegration on the microheater surface cannot be accurately pinpointed in the present experiment. Visual observations show that the bubble disintegrates at most 2 μs before the beginning of bubble regrowth (symbol 'F' in Fig. 3, frame (F) in Fig. 4), which corresponds to a time of 17 μs after the beginning of the heating pulse. According to these observations the results in Fig. 8 and the subsequent figures cover the time period up to 16 μs after the start of the heating pulse.

The growth of the bubble radius (i.e. vapor microlayer characteristic length), bubble wall velocity and

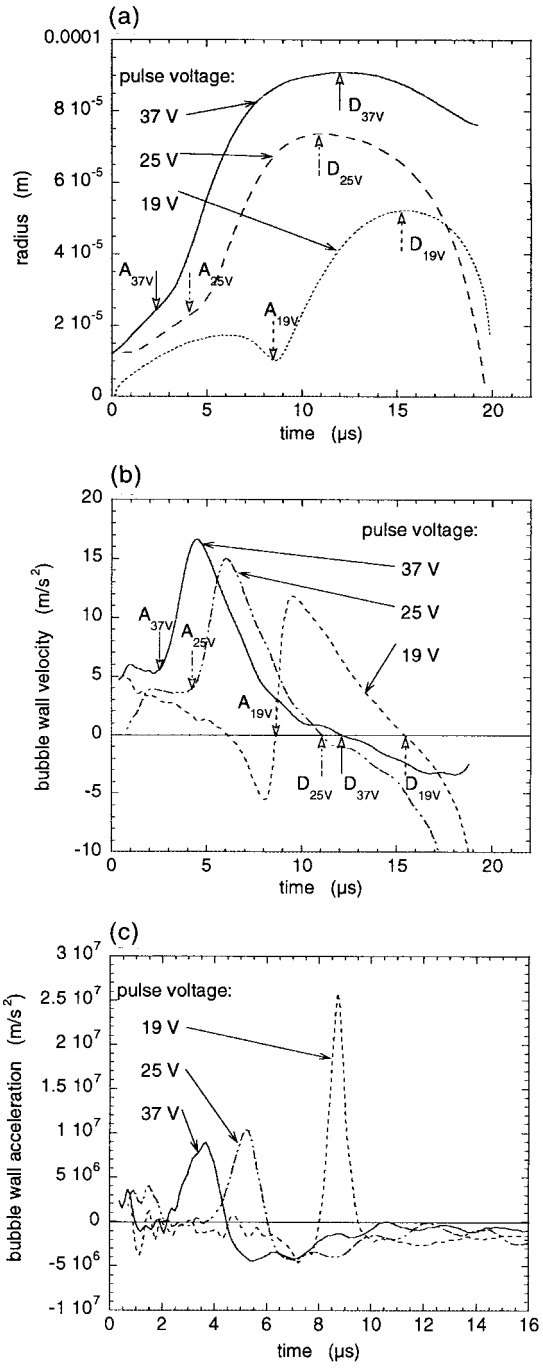

Fig. 9. Bubble wall motion during microscale vapor explosion on a thin film microheater. (a) Bubble radius, (b) bubble wall velocity, (c) bubble wall acceleration under different heating conditions. Heating pulse duration = 6 μs.

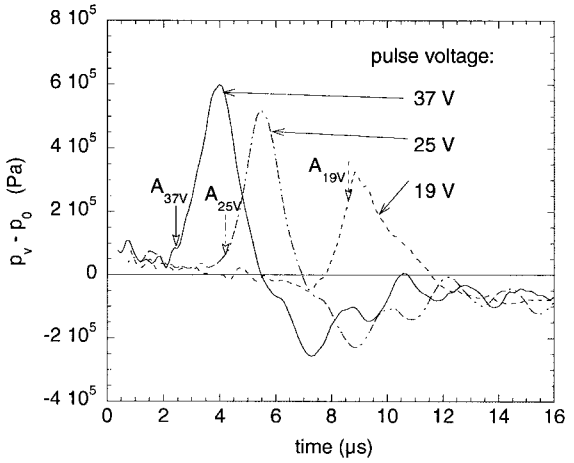

Fig. 10. Vapor microlayer excess pressure at different heating conditions. Heating pulse duration = 6 μs.

acceleration are plotted in Fig. 9. It is immediately clear from Fig. 9(a) that the maximum linear dimension of the vapor bubbles were of the same order as the microheater (~100 μm). The lifetime of the expanding vapor microlayers is about 15 μs. With the increase of applied pulse voltage, the maximum expansion velocity increases, Fig. 9(b). The peak of the bubble expansion velocity reached approximately 17 m/s in the 37 V and 6 μs pulse heating experiment. The bubble wall velocity at the start of the explosive volume growth, indicated by 'A', also increases with the increase of the heating pulse voltage. The bubble wall acceleration is related to the acoustic emission and vapor volume velocity through Eq. (7),

$$\frac{\mathrm{d}^2R}{\mathrm{d}t^2} = \left(\frac{1}{36\pi}\right)^{1/3}\frac{1}{V^{2/3}}\left[\frac{4\pi r}{\rho_1}p_a(t+r/c) - \frac{2}{3V}\left(\frac{\mathrm{d}V}{\mathrm{d}t}\right)^2\right]. \quad (19)$$

Fig. 9(c) shows the effect of the heating pulse magnitude on the peak acceleration of the bubble wall, which is not in phase with the bubble velocity. Note that the time scale of Fig. 9(c) is different than that of Fig. 9(a) and (b).

With the spherical bubble assumption, the bubble excess pressure, $p_v - p_o$, calculated from the Rayleigh–Plesset Eq. (11), is shown in Fig. 10. The maximum excess pressure during the explosive vaporization process increases with the increase of heating pulse voltage. At 37 V, an excess pressure of 6 bars was reached after the initiation of explosive vapor growth. Since the ambient pressure was constant throughout the experiments, the results of Fig. 10 indicate that the pressure within the bubble reaches its maximum after

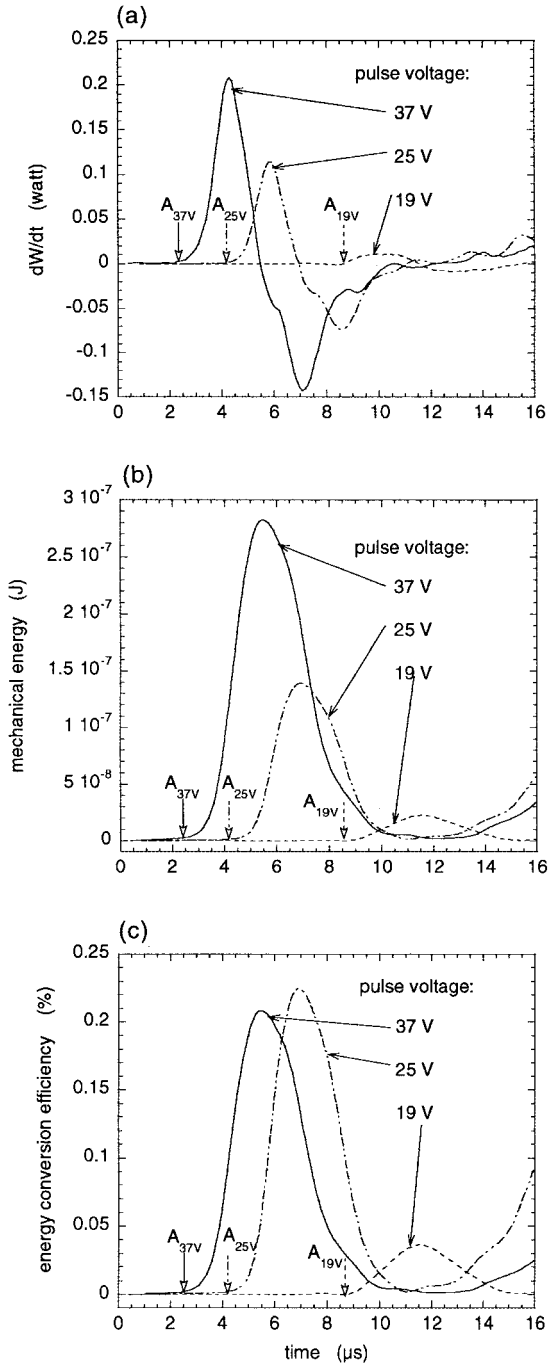

Fig. 11. Energy conversion. (a) Mechanical energy conversion rate, (b) extractable mechanical energy, (c) energy conversion efficiency under different heating conditions. Heating pulse duration = 6 μs.

a time delay from the beginning of the explosive vaporization. The increase of vapor pressure within the vapor phase could only come from either conductive heating of the vapor in contact directly with the microheater surface or rapid vaporization at the vapor/liquid interface. Since the growth rate of thermal diffusion length is proportional to the square root of the diffusion time ($t^{1/2}$), which is slower than the bubble growth rate during explosive growth (t), the increase of pressure inside the bubble after the incipience of the explosive vaporization is a direct consequence of increased vaporization rate at the vapor/liquid interface. Although the exact mechanism that accelerates the vapor production following the onset of vapor explosion is still an open question, recent progress in explosive vaporization research has provided strong evidence that the development of instabilities at the vapor/liquid interface, the Landau instability in particular, is responsible for the interface surface roughening or even for the tearing of the interface at high evaporation rates [45,47–49]. The consequence is a rapid increase of interface area for vaporization that leads to a 'jump' in vaporization rate [47].

In addition to the pressure production, the conversion rate of the supplied electrical energy into the extractable mechanical energy is also important to the application of rapid microbubble generation for micromechanical devices and machines. This information is reported in Fig. 11 according to Eq. (17) together with the amount of extractable mechanical energy calculated from Eq. (16), and the efficiency, $\eta = W/Q$.

As shown in Fig. 11(a), the maximum extractable power was 0.01 W for the 19 V heating pulse condition; it was increased by an order of magnitude, to more than 0.1 W, for the same duration of heating pulse when the voltage was increased to 25 V, which corresponds to the operating condition of the TIJ printer. The peak extractable power was further doubled to more than 0.2 W for the 37 V heating pulse. Obviously, the 19 V heating pulse operating conditions are not appropriate for applications such as thermal ink jet printers, micropumps, and microactuators where the system performance relies on the kinetic energy converted from the input electrical power. Fig. 11(b) shows the corresponding amount of mechanical energy released from the rapid expansion of vapor microlayer for these three heating conditions. It is obvious that substantially higher mechanical energy is produced at higher electrical energy input per pulse. The peak of the extractable mechanical energy is near 0.3 μJ for the 37 V heating pulse. It is also obvious that the mechanical energy is very small prior to the onset of explosive vaporization.

The acoustic conversion efficiency, $\eta_a = E_a/Q$, is calculated using the acoustic energy, E_a, given by Eq. (18). Park et al. [50] calculated the acoustic conversion

in the rapid vaporization of water, on a surface heated by a pulsed laser. The obtained acoustic signal due to the growth of the vapor phase in water is characterized by a single positive pulse. They reported an acoustic conversion efficiency of 0.0015%. To compare with the laser induced acoustic emission in water, the acoustic conversion efficiency is plotted in Fig. 12 for the first positive pulse ($p_a > 0$) of the acoustic waves in Fig. 5. The acoustic conversion efficiency is only 0.0006% for the 19 V heating pulse case; it increases to more than 0.0033% when the heating pulse voltage is increased.

The current acoustic pressure transient measurements have uncertainties due to the quartz pressure transducer resonance at its natural frequency and the charge amplifier linearity error. In the pressure range of the present experiment the uncertainty due to linearity error is about 0.2%. The error caused by the transducer resonance is less than 5% at 1/3 of its natural frequency and increases with the increase of signal frequency. From the pressure signals in Fig. 5, the frequency of the acoustic pressure pulses is in the range of 120–145 kHz. The error increases to less than 10% when the signal frequency is 200 kHz. In the above analysis, integration of Eq. (7) starts from the time $t = r/c$. Electronic circuit noise signals, as can be seen at $t = 0$ in Figs. 3 and 5, will add uncertainties to the vapor volume calculation. Due to the short heating pulse duration, dynamic impedance in the power amplifier and the resistance heating delivery circuits causes uncertainties in the energy input into the microheater.

The distance between the pressure transducer and the microheater is measured by moving the transducer away from the microheater surface after an initial contact between the TIJ chip and the transducer where the distance $x = 0$ is assigned. We estimated that the gap between the microheater surface and the transducer surface at 'contact' can be up to 0.1 mm due to the transducer surface roughness. The precision slide has a measurement accuracy of ± 0.05 mm. For a measured heater-to-sensor-distance of 2 mm, the relative error is 5%.

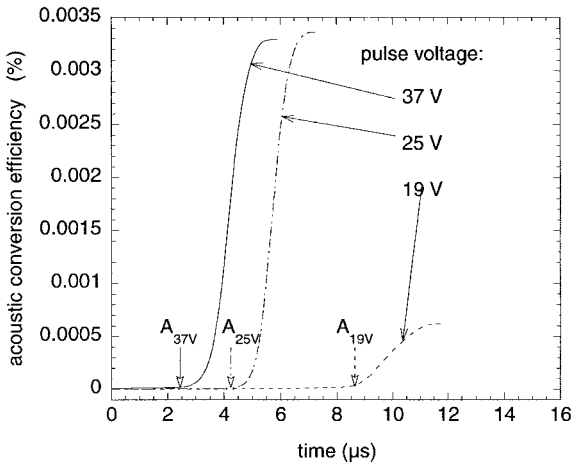

Fig. 12. Acoustic conversion efficiency. Heating pulse duration = 6 μs.

It is important to mount the transducer so that the detection surface is normal to the pressure wave traveling direction. A small deviation from the normal angle of incidence could cause a relatively large reduction in the pressure amplitude and in addition a change in the pulse shape [50]. In the present experiment, the transducer was mounted in the direction resulting in a maximum signal at a given distance from the heater surface. However, experiments performed in a recent study [28] show that for the present setup, deviations of up to 13° from the normal angle of incidence did not lead to a change in pressure amplitude, due to the characteristics of the acoustic sensor. Temperature variation in the range from 20°C to 25°C between experiments also introduces an uncertainty in the measurement of acoustic pressure waves. The water temperature affects density, the travel time of the sound from the source to the sensor, and the amount of heat input to initiate the explosive vaporization process.

Using the quadrature sum of the independent uncertainties [51], the total error of acoustic pressure measurements due to the transducer resonance, the charge amplifier linearity error, and the distance measurement error is 7%. Due to the cumulative nature of vapor volume and velocity calculation which require the integration of acoustic signals, the circuit electronic noise signal will add positive or negative values to the volume calculation, especially at the start and the end of the heating pulse. Integration from the beginning of the acoustic pressure data collection until the arrival of the heating pulse yields an average of noise induced error in volume measurements at the beginning of heating. The maximum value of these errors for all the volume measurements is $\pm 5 \times 10^{-14}$ m^3.

4. Summary

To produce a pressure pulse, thin-film microheaters are operated at heat flux levels several times higher than the theoretical upper limit predicted by Schrage [37]. The acoustic pressure production due to rapid pulse heating of a liquid with a thin-film microheater deposited on a glass substrate is accompanied by a vapor explosion and subsequent implosion. A minimum energy input rate exists for a given duration of heating time below which no explosive vaporization can be realized. The acoustic pressure emission

increases linearly with time shortly after the onset of explosive vaporization. Increasing the rate of energy input to about 15% over the minimum energy input rate needed for explosive vaporization at a given pulse duration will increase the peak value of acoustic pressure production by 500%. Further increase of energy input rate over a range of applied voltage from 20 V to 31 V did not increase the acoustic pressure production. However, the delay time, t_B, between the peak of the generated acoustic pulse and the beginning of heating pulse application decreases monotonically with the increase of heating pulse voltage.

The dynamics of the vapor phase are reconstructed in this paper using either the volume of vapor or a characteristic length (bubble radius) from the data of acoustic pressure measurement. It is clear that the vapor volume is largely generated after the onset of explosive vapor growth. The vapor volume generated from the microscopic vapor explosion has a typical linear dimension on the order of 100 μm, which is about the same as the microheater linear dimension. The maximum expansion velocity of a vapor layer on the microheater surface was 17 m/s in the present experiment. The pressure within the vapor volume was calculated from the Rayleigh–Plesset equation using the vapor volume obtained from the acoustic measurement.

The extractable mechanical energy for explosively expanding vapor microlayer was also calculated. The amount of extractable mechanical energy was approximately 0.3 μJ for the 37 V heating pulse. The corresponding extractable mechanical power was more than 0.2 W. The conversion efficiency from electrical energy into extractable mechanical energy was 0.23% at 25 V heating pulse. The acoustic conversion efficiency was approximately twice that of laser pulse heating induced rapid vaporization of water.

Acknowledgements

The authors acknowledge the helpful discussions with Professor G. Yadigaroglu of the Laboratory of Nuclear Technology at ETH Zurich.

The final preparation of this article was supported in part by the Swiss National Science Foundation (contract number: 2100-052327.97/1).

References

[1] M.I. Corradini, B.J. Kimand, M.D. Oh, Vapor explosions in light water reactors: a review of the theory and modeling, Progress in Nuclear Energy 22 (1) (1988) 1–117.

[2] V.P. Skripov, P.A. Pavlov, Explosive boiling of liquids and fluctuation nucleus formation, High. Temp. (USSR) 8 (1970) 782–787.

[3] K.P. Derewnicki, Experimental studies of heat transfer and vapor formation in fast transient boiling, Int. J. Heat Mass Transfer 28 (1985) 2085–2092.

[4] Y. Iida, K. Okuyama, K. Sakurai, Peculiar bubble generation on a film heater submerged in ethyl alcohol and imposed a high heating rate over 10^7 Ks^{-1}, Int. J. Heat Mass Transfer 36 (1994) 2699–2701.

[5] A. Asai, S. Hirasawa, I. Endo, Bubble generation mechanism in the bubble jet recording process, Journal of Imaging Technology 14 (1988) 120–124.

[6] T. Asshauer, K. Rink, G. Delacrétaz, Acoustic transient generation by holmium laser induced cavitation bubbles, Journal of Applied Physics 76 (1994) 5007–5013.

[7] H.K. Park, D. Kim, C.P. Grigoropoulos, C.C. Poon, A.C. Tam, Optical measurements of pressure transients in the rapid vaporization of liquids on a pulsed-laser-heated surface, in: Proceedings of the ASME Heat Transfer Division HTD-Vol 317-2, IMECE, 1995, pp. 391–398.

[8] D. Kim, C.P. Grigoropoulos, Pulsed laser-induced ablation of absorbing liquids and acoustic–transient generation, IMECE HTD-Vol 351 (1997) 45–54.

[9] Q. Lu, D.B. Wallace, D.J. Hayes, High-speed photographic studies of dye-assisted pulsed Nd: YAG laser ablation of dental hard tissues, SPIE 2975 (1997) 396–407.

[10] A. Asai, T. Hara, I. Endo, One-dimensional model of bubble growth and liquid flow in bubble jet printers, Japanese Journal of Applied Physics 26 (1987) 1794–1801.

[11] R.R. Allen, J.D. Meyer, W.R. Knight, Thermodynamics and hydrodynamics of thermal ink jets, Hewlett-Packard Journal 5 (1985) 21–27.

[12] I. Rezanka, Thermal ink jet-a review, Proceedings SPIE 1670 (1992) 192–200.

[13] A. Asai, Three-dimensional calculation of bubble growth and drop ejection in a bubble jet printer, ASME Journal of Fluids Engineering 114 (1992) 638–641.

[14] A. Asai, Bubble dynamics in boiling under high heat flux pulse heating, ASME J. Heat Transfer 113 (1991) 973–979.

[15] A. Asai, Application of the nucleation theory to the design of bubble jet printers, Japanese Journal of Applied Physics 28 (1989) 909–915.

[16] W. Runge, Nucleation in thermal ink-jet printers, IS&T's Eight International Congress on Advances in Non-Impact Printing Technologies (1992) 299–302.

[17] P. Chen, W. Chen, S-H. Chang, Bubble growth and ink ejection process of a thermal in jet printhead, Int. J. Mech. Sci. 39 (1997) 638–695.

[18] J.R. Maa, C.Y. Tung, The maximum boiling superheat of water, Letters in Heat and Mass Transfer 7 (1980) 121–128.

[19] I. Owen, J.M. Jalil, Heterogeneous flashing in water drops, Int. Journal of Multiphase Flow 17 (5) (1991) 653–660.

[20] P. Reinke, Surface Boiling of Superheated Liquid, Ph.D. thesis, No. 11598, Swiss Federal Institute of Technology (ETH), Zürich, Switzerland, 1996.

[21] V.P. Skripov, Metastable Liquids, John Wiley, New York, 1974, Chs 4 and 6.
[22] E.V. Bhaskar, J.S. Aden, Development of the thin-film structure for the ThinkJet Printhead, Hewlett-Packard Journal 5 (1985) 27–33.
[23] M. Sakurai, M. Kawaharada, M. Tsuzuki, Dynamic analysis of vapor bubble in liquid using acoustic emission measurement, Japanese Journal of Applied Physics 27 (Suppl. 27-1) (1988) 79–81.
[24] J.D. Meyer, Bubble growth and nucleation properties in thermal ink-jet printing technology, SID 86 Digest (1986) pp. 101–104.
[25] H. McCann, L.J. Clarke, P.A. Masters, An experimental study of vapor growth at the superheat limit temperature, Int. J. Heat Mass Transfer 32 (6) (1989) 1077–1093.
[26] A. Lesin, H. Baron, H. Branover, J.C. Merchuk, Direct contact boiling at the superheat limit, in: Proceedings of the Tenth International Heat Transfer Conference 3, 1994, pp. 347–352.
[27] M. Strasberg, Gas bubbles as sources of sound in liquids, J. Acoust. Soc. Am. 28 (1956) 20–26.
[28] N. Bieri, Untersuchung der Entstehung von Dampfblasen auf einer Dünnfilm-Mikroheizung, Visualisierung und Druckmessung, Semesterarbeit, ETH, Zürich, Switzerland, 1998.
[29] L. Rayleigh, On the pressure developed in a liquid during the collapse of a spherical cavity, Philosophical Magazine 34 (199) (1917) 94–98.
[30] P.A. Pavlov, V.P. Skripov, Boiling of a liquid with pulsed heating: 1. Hot-wire method of experiment, High Temp. (USSR) 3 (1965) 97–101.
[31] P.A. Pavlov, V.P. Skripov, Kinetics of spontaneous nucleation in strongly heated liquids, High Temp. (USSR) 8 (1970) 540–545.
[32] V.P. Skripov, P.A. Pavlov, E.N. Sinitsyn, Heating of liquids to boiling by a pulsating heat supply: 2. Experiments with water, alcohols, n-hexane and nonane, High Temp. (USSR) 3 (1965) 670–674.
[33] Y. Iida, K. Okuyama, K. Sakurai, Boiling nucleation on a very small film heater subjected to extremely rapid heating, Int. J. Heat Mass Transfer 37 (1994) 2771–2780.
[34] K. Okuyama, Y. Iida, Transient boiling heat transfer characteristics of nitrogen (bubble behavior and heat transfer rate at stepwise heat generation), Int. J. Heat Mass Transfer 33 (1990) 2065–2071.
[35] J. Pöppel, Sensor- und aktoreigenschaften von bubble-jet-heizelementen in tintenschreibwerken, Dissertation, München, 1991.
[36] S. Glod, Bubble Dynamics on a Thin Film Microheater, Diplomarbeit, ETH, Zürich, Switzerland, 1997.
[37] R.W. Schrage, A Theoretical Study of Interphase Mass Transfer, Columbia University Press, New York, 1953, Ch. 3.
[38] V.P. Carey, Liquid–Vapor Phase-Change Phenomena, Hemisphere, London, 1992, pp. 112–124, 138–150.
[39] F.P. Incropera, D.P. DeWitt, Table A 6, in: Introduction to Heat Transfer, 3rd ed., Wiley, New York, 1996, p. 239.
[40] M.S. Plesset, A. Prosperetti, Bubble dynamics and cavitation, Ann. Rev. Fluid Mech. 9 (1977) 145–185.
[41] F.R. Young, Cavitation, McGraw Hill, London, 1989, Ch. 2.
[42] L.D. Landau, E.M. Lifshitz, Fluid Mechanics, 2nd ed., Pergamon Press, Oxford, 1993, pp. 251–283.
[43] C.E. Brennen, Cavitation and Bubble Dynamics, Oxford University Press, New York, 1995, Ch. 2.
[44] D. Ross, Mechanics of Underwater Noise, Pergamon Press, New York, 1976, pp. 35–36, 51–52.
[45] J.E. Shepherd, B. Sturtevant, Rapid evaporation at the superheat limit, J. Fluid Mechanics 121 (1982) 379–402.
[46] D.L. Frost, Dynamics of explosive boiling of a droplet, Phys. Fluids 31 (9) (1988) 2554–2561.
[47] D.L. Frost, B. Sturtevant, Effects of ambient pressure on the instability of a liquid boiling explosively a the superheat limit, ASME J. Heat Transfer 108 (1986) 418–424.
[48] H.S. Lee, H. Merte, The origin of the dynamic growth of vapor bubbles related to vapor explosions, ASME J. Heat Transfer 120 (1998) 174–182.
[49] D. Juric, On the interface instability during rapid evaporation in microgravity, Micro-Electro-Mechanical Systems (MEMS) DSC-Vol 62 (1997) 101–104 HTD-Vol. 354.
[50] D.K.H.K. Park, C.P. Grigoropoulos, A.C. Tam, Pressure generation and measurement in the rapid vaporization of water on a pulsed-laser-heated surface, J. Applied Physics 80 (7) (1996) 4072–4081.
[51] J.R. Taylor, An Introduction to Error Analysis, University Science Books, Mill Valley, CA, 1982, Ch. 3.